

FIRST RESULT OF THE EXPERIMENTAL SEARCH
FOR THE 9.4 keV SOLAR AXION REACTIONS WITH
 ^{83}Kr IN THE COPPER PROPORTIONAL COUNTER

*Yu. M. Gavriluk*¹, *A. M. Gangapshev*^{1,*}, *A. V. Derbin*²,
*V. V. Kazalov*¹, *H. J. Kim*⁵, *Y. D. Kim*⁶, *V. V. Kobychiev*⁴,
*V. V. Kuzminov*¹, *Luqman Ali*⁵, *V. N. Muratova*²,
S. I. Panasenko^{1,3}, *S. S. Ratkevich*^{1,3}, *D. A. Semenov*²,
*D. A. Tekueva*¹, *S. P. Yakimenko*¹, *E. V. Unzhakov*²

¹ Institute for Nuclear Research, RAS, Moscow

² Petersburg Nuclear Physics Institute, St. Petersburg, Russia

³ Kharkov National University, Kharkov, Ukraine

⁴ Institute for Nuclear Research of NAS Ukraine, Kiev

⁵ Department of Physics, Kyungpook National University, Daegu, Republic of Korea

⁶ Institute of Basic Science, Daejeon, Republic of Korea

The experimental search for solar hadronic axions started at the Baksan Neutrino Observatory of the Institute for Nuclear Research, Russian Academy of Sciences (BNO INR RAS). It is assumed that axions are created in the Sun during $M1$ transition between the first thermally excited level at 9.4 keV and the ground state in ^{83}Kr . The experiment is based on axion detection via resonant absorption process by the same nucleus in the detector. The big copper proportional counter filled with krypton is used to detect signals from axions. The experimental setup is situated in the deep underground low-background laboratory. No evidences of axion detection were found after the 26.5 days data collection. Resulting new upper limit on axion mass is $m_A \leq 130$ eV at 95% C.L.

PACS: 14.80.Va; 26.65.+t

INTRODUCTION

A solution of the strong CP problem based on the global chiral symmetry $U(1)$ was proposed by Peccei and Quinn (PQ) [1]. The existence of the axions was predicted by Weinberg [2] and Wilczek [3] as a result of spontaneous breaking of the PQ symmetry at the energy f_A . The axion mass (m_A) and the strength

*E-mail: gangapsh@list.ru

of an axion's coupling to an electron (g_{Ae}), a photon ($g_{A\gamma}$), and nucleons (g_{AN}) are proportional to the inverse of f_A . At the moment, there are two classes of models for the axion: the hadronic axion (KSVZ-model) [4] and GUT axion (DFSZ-model) [5]. The axion mass in both models is defined as

$$m_A = \frac{f_\pi m_\pi}{f_A} \left(\frac{z}{(1+z+w)(1+z)} \right), \quad (1)$$

where $f_\pi \simeq 93$ MeV — pion decay constant; $z = m_u/m_d \simeq 0.56$ and $w = m_u/m_s \simeq 0.029$ — quark-mass ratios. It gives $m_A[\text{eV}] \simeq 6.0 \cdot 10^6/f_A[\text{GeV}]$.

The main difference between models is that in contrast to the DFSZ-model, in KSVZ-model axions have no coupling to leptons and ordinary quarks at the tree level. As a result, the interaction of the KSVZ axion with electrons through radiatively induced coupling is strongly suppressed [6].

If axions do exist, then the Sun and other stars should be an intense source of these particles. In 1991, Haxton and Lee calculated the energy loss of stars along the red-giant and horizontal branches due to the axion emission in nuclear magnetic transitions in ^{57}Fe , ^{55}Mn , and ^{23}Na nuclei [7]. In 1995, Moriyama proposed experimental scheme to search for 14.4 keV monochromatic solar axions that would be produced when thermally excited ^{57}Fe nuclei in the Sun relax to its ground state and could be detected via resonant excitation of the same nuclide in a laboratory [8]. Searches for resonant absorption of solar axions emitted in the nuclear magnetic transitions were performed with ^{57}Fe [9–14], ^7Li [15–17], and ^{83}Kr [18] nuclei.

In this paper, we present the results of the search for solar axions using the resonant absorption by ^{83}Kr nuclei. The energy of the first excited $7/2^+$ nuclear level is equal to 9.405 keV, lifetime $\tau = 2.23 \cdot 10^{-7}$ s, internal conversion coefficient $\alpha = 17.0$, and the mixing ratio of 17 and 17' transitions is $\delta = 0.013$ [19].

In accordance with indirect estimates, the abundance of the krypton in the Sun (Kr/H) = 1.78×10^{-9} atom/atom [20] that corresponds to $N = 9.08 \cdot 10^{13}$ of ^{83}Kr atom per 1 g material in the Sun.

To estimate axion flux from the Sun, the calculation can be performed as in [7]. The axion flux from a unit mass is equal to

$$\delta\Phi(T) = N \frac{2 \exp(-\beta_T)}{1 + 2 \exp(-\beta_T)} \frac{1}{\tau_\gamma} \frac{\omega_A}{\omega_\gamma}, \quad (2)$$

where N — number of ^{83}Kr atoms in 1 g of material in the Sun; $\beta_T = E_\gamma/kT$; τ_γ — lifetime of the nuclear level; ω_A/ω_γ represents the branching ratio of axions to photon emission. The ratio ω_A/ω_γ was calculated in [7, 21, 22] as

$$\frac{\omega_A}{\omega_\gamma} = \frac{1}{2\pi\alpha} \frac{1}{1 + \delta^2} \left[\frac{g_0\beta + g_3}{(\mu_0 - 0.5)\beta + \mu_3 - \eta} \right]^2 \left(\frac{p_A}{p_\gamma} \right)^3, \quad (3)$$

where μ_0 and μ_3 — isoscalar and isovector magnetic moments; g_0 and g_3 — isoscalar and isovector parts of the axion–nucleon coupling constant g_{AN} ; and β and η — nuclear structure-dependent terms.

In the case of the ^{83}Kr nucleus, which has the odd number of nucleons and an unpaired neutron, in the one-particle approximation the values of β and η can be estimated as $\beta \approx -1.0$ and $\eta \approx 0.5$.

In the hadronic axion models, the g_0 and g_3 constants can be represented in the form [6]:

$$g_0 = -\frac{m_N}{6f_A} \left[2S + (3F - D) \frac{1 + z - 2w}{1 + z + w} \right], \quad (4)$$

$$g_3 = -\frac{m_N}{2f_A} \left[(D + F) \frac{1 - z}{1 + z + w} \right], \quad (5)$$

where D and F denote the reduced matrix elements for the $SU(3)$ octet axial vector currents, and S characterizes the flavor singlet coupling [6]. The parameter S characterizing the flavor singlet coupling still remains a poorly constrained one [14]. The most stringent boundaries ($0.37 \leq S \leq 0.53$) and ($0.15 \leq S \leq 0.5$) were found in [23] and [24], accordingly.

The axion flux was calculated for the standard solar model BS05 [25] characterized by a high metallicity [26]. The differential flux at the maximum of the distribution (6) is

$$\Phi_A(E_{M1}) = 5.97 \cdot 10^{23} \left(\frac{\omega_A}{\omega_\gamma} \right) \text{ cm}^{-2} \cdot \text{s}^{-1} \cdot \text{keV}^{-1}. \quad (6)$$

The width of the resulting distribution, which is described well by a Gaussian curve, is $\sigma = 1.2$ eV. This value exceeds substantially the recoil-nucleus energy and the intrinsic and Doppler widths of the level of ^{83}Kr target nuclei.

The cross section for resonance axion absorption is given by an expression similar to the expression for the photon-absorption cross section, the correction for the ratio ω_A/ω_γ being taken into account,

$$\sigma(E_A) = 2\sqrt{\pi}\sigma_{0\gamma} \exp \left[-\frac{4(E_A - E_M)^2}{\Gamma^2} \right] \left(\frac{\omega_A}{\omega_\gamma} \right), \quad (7)$$

where $\sigma_{0\gamma} = 1.22 \cdot 10^{-18} \text{ cm}^2$ is the maximum cross section of the γ -ray resonant absorption and $\Gamma = 1/\tau$. The total cross section for axion absorption can be obtained by integrating $\sigma(E_A)$ over the axion spectrum. The expected rate of resonance axion absorption by the ^{83}Kr nucleus as a function of the probability for axion emission ω_A/ω_γ ; the parameter $(g_3 - g_0)$, which describes axion–nucleon interaction; and the axion mass in the KSVZ model can be represented

in the form ($S = 0.5$, $z = 0.56$):

$$R_A[\text{g}^{-1} \cdot \text{day}^{-1}] = 4.23 \cdot 10^{21} (\omega_A/\omega_\gamma)^2, \quad (8)$$

$$= 8.53 \cdot 10^{21} (g_3 - g_0)^4 (p_A/p_\gamma)^6, \quad (9)$$

$$= 2.41 \cdot 10^{-10} (m_A)^4 (p_A/p_\gamma)^6. \quad (10)$$

The number of detected photons following axion absorption is determined by the target mass, measurement time, and detector efficiency. At the same time, the probability of observing a peak at 9.4 keV depends on the background level in the experimental facility used.

1. EXPERIMENTAL SETUP

The experimental technics is based on registration of the γ -quantum and conversion electrons appearing after deexcitation of the ^{83}Kr nuclei. To register this process, a large proportional counter (LPC) with a casing of copper is used. The gas mixture $\text{Kr}(99.55\%) + \text{Xe}(0.45\%)$ is used as working media of the LPC. The isotopic composition of the krypton is: $^{78}\text{Kr}(0.002\%) + ^{80}\text{Kr}(0.411\%) + ^{82}\text{Kr}(41.355\%) + ^{83}\text{Kr}(58.229\%) + ^{84}\text{Kr}(0.003\%)$. The LPC is a cylinder with inner and outer diameters of 137 and 150 mm, respectively. A gold-plated tungsten wire of 10 μm in diameter is stretched along the LPC axis and is used as an anode. To reduce the influence of the counter edges on the operating characteristics of the counter, the end segments of the wire are passed through the copper tubes (3 mm in diameter and 38.5 mm in length) electrically connected to the anode. These segments operate as an ionization chamber with no gas amplification. Taking into account teflon insulators dimensions, the distance from operation region to the flange is 70 mm. The fiducial length of the LPC is 595 mm, and the corresponding volume is 8.77 l. Gas pressure is 5.6 bar, and corresponding mass of the ^{83}Kr -isotope in fiducial volume of the LPC is 101 g.

The LPC is surrounded by passive shield made of copper (~ 20 cm), lead (~ 20 cm), and polyethylene (8 cm). The setup is located in the Deep Underground Low-Background Laboratory at BNO INR RAS [27], at the depth of 4700 m w.e., where the cosmic ray flux is reduced by $\sim 10^7$ times in comparison to that above ground, and evaluated as $(3.0 \pm 0.1) \cdot 10^{-9} \text{ cm}^{-2} \cdot \text{s}^{-1}$ [28].

The detector signals are passed from one end of the anode wire to the charge-sensitive preamplifier. A total shape of pulses (waveforms) are recorded by the digitizer after amplification in an auxiliary amplifier. A digital oscilloscope LAn-n20-12USB integrated with a computer via USB-port is used. Sampling frequency is 12.5 MHz and record window is 2048 bins (164 μs). Sample of the recorded waveform is presented in Fig. 1, *a*. There is a feature in the waveforms, namely, the presence of secondary pulse after the primary pulse. Those secondary pulses are the result of photoemission from the cathode. Photons appear near

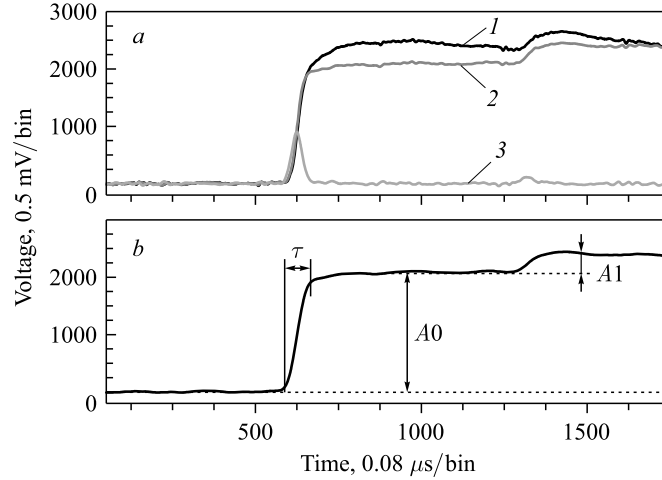


Fig. 1. *a*) Samples of recorded pulse (1), electronic current (3) and corrected pulse (2); *b*) schematic description of the parameters of the corrected pulses used for data analysis. A_0 — amplitude of the primary pulse; A_1 — amplitude of the secondary pulse; τ — pulse rise time

anode wire in time of the development of an electron avalanche from the primary ionization electrons. The relative height of the secondary pulse depends on the position of the events along anode wire due to the changing of a cathode view solid angle. The lowest value of the angle is reached at the ends of the anode wire and the smallest secondary pulses appeared as a result. Recorded waveforms are processed to define parameters of the events. First of all, the response function of the LPC for single electron of the primary ionization is used to define the electron density profile for the given event (electron current). The shape of the response function is defined as

$$V(t) = a \cdot \exp\left(-\frac{t+B1}{\tau}\right) \left(\log\left(1+\frac{t}{B}\right) + \frac{t}{\tau} + \frac{t^2}{8\tau^2}\right) \cos\left(\frac{2\pi t}{T}\right), \quad (11)$$

where $T = 460 \mu s$, $B = 2.4 \cdot 10^{-3} \mu s$ and $\tau = 240 \mu s$. The cumulative sum (integral) of the electronic current is a corrected waveform as in [29]. Samples of the recorded electronic current and the corrected waveform are presented in Fig. 1, *a*. Schematic description of the used parameters is presented in Fig. 1, *b*. The amplitude of the secondary pulse is used to define the relative position of the events along the anode wire by the ratio:

$$\lambda = 1000 \frac{A_1}{A_0}, \quad (12)$$

where A_1 — amplitude of the secondary pulse; A_0 — amplitude of the primary pulse (see Fig. 1, *b*).

2. RESULTS

The background spectra collected during 26.5 days and fit result curve are presented in Fig. 2. Fitting function is taken as

$$f(x) = 7151 \exp \left[- \left(\frac{x - 134.6}{9.567} \right)^2 \right] + 886.4 \exp \left[- \left(\frac{x - 119.1}{16.64} \right)^2 \right] + 130.7 \exp \left[- \left(\frac{x - 85.72}{12.00} \right)^2 \right] + 81.40 \left(1.57 - \arctan \left(\frac{x - 123.4}{1.716} \right) \right) + 10.88 \exp \left[- \left(\frac{x}{569.6} \right) \right] + 5.596. \quad (13)$$

The peak of 13.5 keV from K -capture of ^{81}Kr is well seen. ^{81}Kr is a cosmogenic isotope. It is present as a trace admixture in the used samples of krypton. This isotope is produced in atmosphere mainly in reactions $^{82}\text{Kr}(n, 2n)^{81}\text{Kr}$ and $^{80}\text{Kr}(n, \gamma)^{81}\text{Kr}$, the half-life time is $T_{1/2} = 2.1 \cdot 10^5$ y. There are two more peaks: ~ 12 and ~ 8 keV. The peak near 12 keV is produced by events, where the K -capture of ^{81}Kr happens near the end of the counter (out of the fiducial volume) and the characteristic photon of daughter nuclide ^{81}Br is registered in the fiducial volume ($K_{\alpha 1} = 11.923$ keV (57.1%), $K_{\alpha 2} = 11.877$ keV (29.1%), $K_{\beta 1} = 13.290$ keV (12.7%), $K_{\beta 2} = 13.465$ keV (1.0%) [30]). The peak near 8 keV is produced by characteristic photons from the copper ($K_{\alpha 1} = 8.047$ keV (58.4%), $K_{\alpha 2} = 8.027$ keV (29.8%), $K_{\beta 1} = 8.904$ keV (11.7%) [30]). The distributions of the events versus pulse rise time and parameter λ are presented in

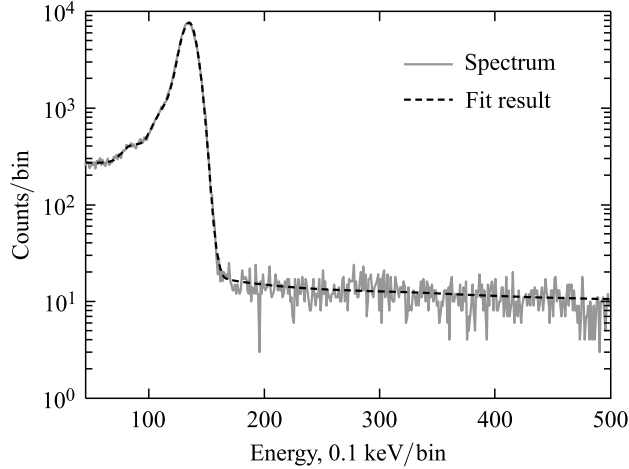


Fig. 2. Background spectra collected with LPC during 26.5 days of measurements and fitting function (13)

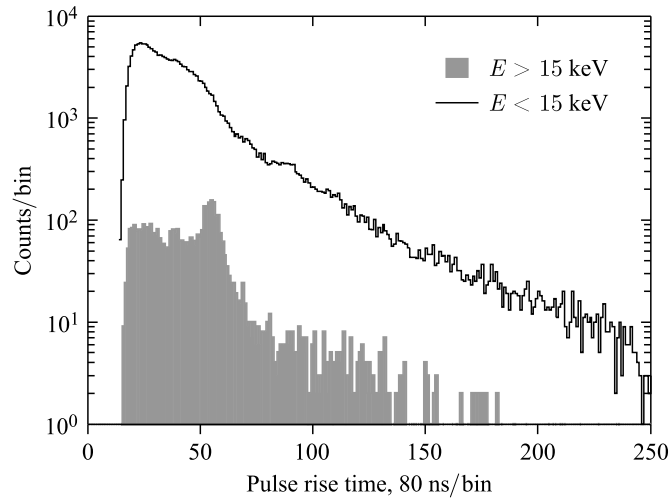
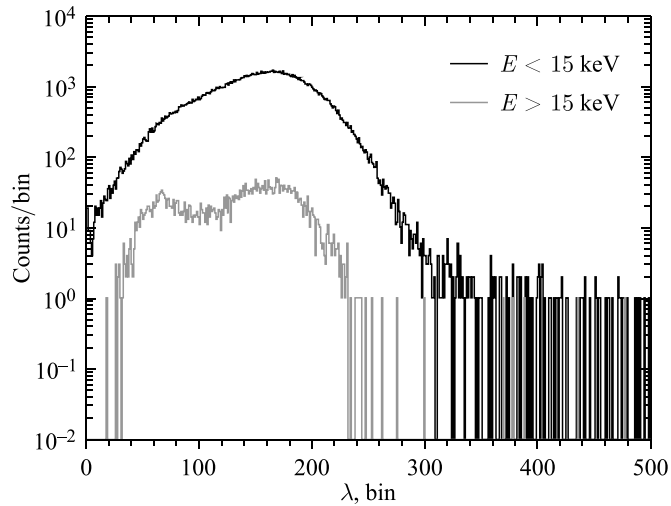


Fig. 3. Distribution of the events versus pulse rise time

Fig. 4. Distribution of the events versus λ

Figs. 3 and 4, respectively. The events with pulse rise time of $\simeq 55$ bins ($4.4 \mu\text{s}$) mostly are the single site events from the inner surface of the cathode (well seen in the distribution for the events with $E > 15.0$ keV). The pulses with longer pulse rise time are mostly the multisite events. The events with $\lambda < 115$ are mostly close to the edge of the fiducial volume (events in the peak of $\simeq 12$ keV) or out of it (high energy events at the ends of the counter, without gas amplification).

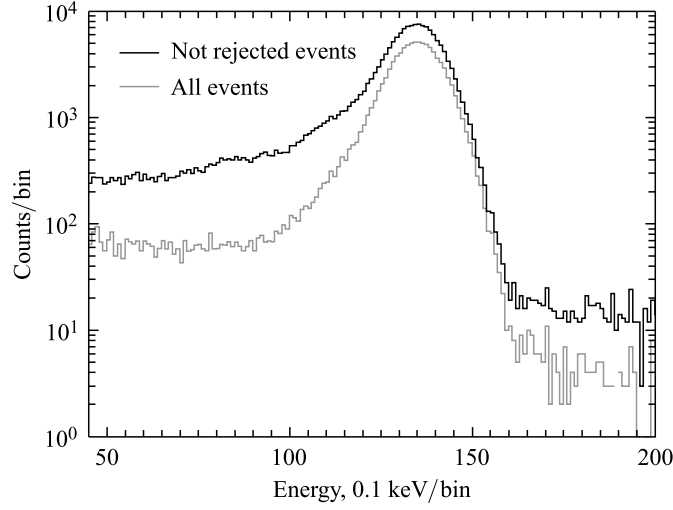


Fig. 5. Original energy spectrum and spectrum after rejection of the events with pulse rise time longer than 47 bins ($3.8 \mu\text{s}$) and λ lower than 115

Thus, as we are looking for single site events in the inner volume of the detector, the events with pulse rise time longer than 47 bins ($3.8 \mu\text{s}$) and λ lower than 115 are rejected. The resulting spectrum in comparison with original one is presented in Fig. 5. There is no visible peak around 9.4 keV from axions. Region of interest is 8.2–9.4 keV, where should be 47.5% of axion events. Detection efficiencies after applying energy cut, pulse rise time cut, and λ cut are $\varepsilon_E = 0.475$, $\varepsilon_\tau = 0.94$, $\varepsilon_\lambda = 0.91$, respectively. The number of events in the region of interest after cuts applying is equal to 703 cts. As there is no “signal” from axions, the upper limit on excitation rate of ^{83}Kr by solar hadronic axions in the detector is defined as

$$R_{\text{exp}} \leq \frac{2\sqrt{2B}}{m_{\text{Kr}} t_{\text{meas}} \varepsilon_E \varepsilon_\tau \varepsilon_\lambda} = 0.069 [\text{g}^{-1} \cdot \text{day}^{-1}], \quad (14)$$

where B — background in the region of interest; m_{Kr} — the mass of the ^{83}Kr (gram); t_{meas} — measurement time (day).

Relation (14) obtained in the experiment limits the region of possible values of the coupling constants g_0 , g_3 and axion mass m_A . In accordance with Eqs. (8)–(10), and on condition that $(p_A/p_\gamma) \cong 1$ provided for $m_A < 3 \text{ keV}$, one can obtain

$$|g_3 - g_0| \leq 1.69 \cdot 10^{-6}, \text{ and} \quad (15)$$

$$m_A \leq 130 \text{ eV} \text{ at } 95\% \text{ C.L.} \quad (16)$$

The limit (16) is stronger than the constraint obtained with 14.4 keV ^{57}Fe solar axions — ($m_A \leq 145$ eV [14]) and is significantly stronger than previous result obtained in ^{83}Kr experiment [18].

CONCLUSION

A search for resonant absorption of the solar axion by ^{83}Kr nuclei was performed using the proportional counter installed inside the low-background setup at the Baksan Neutrino Observatory. The intensity of the 9.4 keV peak measured for 26.5 days turned out to be ≤ 7.0 events/day. The obtained model-independent upper limit on axion–nucleon couplings allowed us to set the new upper limit on the hadronic axion mass of $m_A \leq 130$ eV (95% C.L.) with the generally accepted values $S = 0.5$ and $z = 0.56$. The obtained limit on axion mass strongly depends on the exact values of the parameters S and z .

The work is supported by Russian Foundation of Basic Research (Grants No.14-02-00258A, 13-02-01199A, and 13-02-12140-ofi-m). V. V. Kobychiev is supported in part by the Space Research Program of NAS, Ukraine.

REFERENCES

1. *Peccei R. D., Quinn H. R.* Constraints Imposed by CP Conservation in the Presence of Instantons // *Phys. Rev. D.* 1977. V. 16. P. 1791.
2. *Weinberg S.* A New Light Boson? // *Phys. Rev. Lett.* 1978. V. 40. P. 223.
3. *Wilczek F.* Problem of Strong p and t Invariance in the Presence of Instantons // *Ibid.* P. 279.
4. *Kim J. E.* Weak Interaction Singlet and Strong CP Invariance // *Phys. Rev. Lett.* 1979. V. 43. P. 103;
Shifman M. A., Vainstein A. I., Zakharov V. I. Can Confinement Ensure Natural CP Invariance of Strong Interactions? // *Nucl. Phys. B.* 1980. V. 166. P. 493.
5. *Zhitnitskii A. R.* On Possible Suppression of the Axion Hadron Interactions // *Yad. Fiz.* 1980. V. 31. P. 497;
Dine M., Fischler F., Srednicki M. A Simple Solution to the Strong CP Problem with a Harmless Axion // *Phys. Lett. B.* 1981. V. 104. P. 199.
6. *Srednicki M.* Axion Couplings to Matter. 1. CP Conserving Parts // *Nucl. Phys. B.* 1985. V. 260. P. 689;
Kaplan D. B. Opening the Axion Window // *Ibid.* P. 215.
7. *Haxton W. C., Lee K. Y.* Red Giant Evolution, Metallicity and New Bounds on Hadronic Axions // *Phys. Rev. Lett.* 1991. V. 66. P. 2557.
8. *Moriyama S.* A Proposal to Search for a Monochromatic Component of Solar Axions Using ^{57}Fe // *Phys. Rev. Lett.* 1995. V. 75 P. 3222.
9. *Krcmar M. et al.* Search for Invisible Axions Using ^{57}Fe // *Phys. Lett. B.* 1998. V. 442. P. 38.

10. *Derbin A. V. et al.* Search for Resonant Absorption of Solar Axions Emitted in an $M1$ Transition in ^{57}Fe Nuclei // JETP Lett. 2007. V. 85. P. 12.
11. *Namba T.* Results of a Search for Monochromatic Solar Axions Using ^{57}Fe // Phys. Lett. B. 2007. V. 645. P. 398.
12. *Derbin A. V. et al.* Search for Resonant Absorption of Solar Axions Emitted in $M1$ Transition in ^{57}Fe Nuclei // Eur. Phys. J. C. 2009. V. 62. P. 755.
13. *Danevich F. A. et al.* Heat Flow of the Earth and Resonant Capture of Solar ^{57}Fe Axions // Kinematics and Physics of Celestial Bodies. 2009. V. 25. P. 102.
14. *Derbin A. V. et al.* New Limit on the Mass of 14.4-keV Solar Axions Emitted in an $M1$ Transition in ^{57}Fe Nuclei // Phys. At. Nucl. 2011. V. 74. P. 596.
15. *Krcmar M. et al.* Search for Solar Axions Using Li-7 // Phys. Rev. D. 2001. V. 64. P. 115016.
16. *Derbin A. V. et al.* Search for Solar Axions Emitted in an $M1$ Transition in Li-7 Nuclei // JETP Lett. 2005. V. 81. P. 365.
17. *Belli P. et al. (DAMA Collab.)*. Search for Li-7 Solar Axions Using Resonant Absorption in LiF Crystal: Final Results // Phys. Lett. B. 2012. V. 711. P. 41.
18. *Jakovcic K. et al.* A Search for Solar Hadronic Axions Using Kr-83 // Rad. Phys. Chem. 2004. V. 71. P. 93; arXiv:nucl-ex/0402016v1.
19. *Wu S. C.* // Nuclear Data Sheets. 2001. V. 92 P. 893.
20. *Asplund M. et al.* The Chemical Composition of the Sun // Ann. Rev. Astron. Astrophys. 2009. V. 47. P. 481; arXiv:0909.0948.
21. *Donnelly T. W. et al.* Do Axions Exist? // Phys. Rev. D. 1978. V. 18. P. 1607.
22. *Avignone F. T. et al.* Search for Axions from the 1115-keV Transition of ^{65}Cu // Phys. Rev. D. 1988. V. 37. P. 618.
23. *Faeldt G., Pilkuhn H.* Inner Coulomb Corrections to Pion–Nucleus Scattering // Phys. Lett. B. 1997. V. 46. P. 337.
24. *Adams D. et al. (Spin Muon Collab.)*. Spin Structure of the Proton from Polarized Inclusive Deep Inelastic Muon–Proton Scattering // Phys. Rev. D. 1997. V. 56. P. 5330.
25. *Bahcall J. H., Serenelli A. M., Basu S.* New Solar Opacities, Abundances, Helioseismology, and Neutrino Fluxes // Astrophys. J. 2005. V. 621. P. L85.
26. *Grevesse N., Sauval A. J.* Standard Solar Composition // Space Sci. Rev. 1998. V. 85. P. 161.
27. *Gavriljuk Yu. M. et al.* Working Characteristics of the New Low-Background Laboratory (DULB-4900, Baksan Neutrino Observatory) // Nucl. Instr. Meth. A. 2013. V. 729. P. 576.
28. *Gavrin V. N. et al.* Preprint INR RAS. 1991. P. 698.
29. *Gavrilyuk Yu. M. et al.* Pulse Shape Analysis and Identification of Multipoint Events in a Large-Volume Proportional Counter in an Experimental Search for $2K$ Capture Kr-78 // Instr. Exp. Tech. 2010. V. 53. P. 57; *Gavrilyuk Yu. M. et al.* // Phys. Rev. C. 2013. V. 87. P. 035501.
30. *Blokhin M. A., Shveizer I. G.* Rentgenospektralniy Spravochnik. M.: Nauka, 1982 (in Russian).